

Learning Spatiotemporal Occupancy Grid Maps for Lifelong Navigation in Dynamic Scenes

Hugues Thomas

University of Toronto, Canada
hugues.thomas@utoronto.ca

Matthieu Gallet de Saint Aurin

ETH Zürich, Switzerland
maaurin@student.ethz.ch

Jian Zhang

Apple Inc, United States
jianza@apple.com

Timothy D. Barfoot

University of Toronto, Canada
tim.barfoot@utoronto.ca

Abstract: We present a novel method for generating, predicting, and using Spatiotemporal Occupancy Grid Maps (SOGM), which embed future information of dynamic scenes. Our automated generation process creates groundtruth SOGMs from previous navigation data. We use them to train a 3D-2D feedforward architecture, in a self-supervised fashion, thus enabling lifelong learning for robots. The automated generation process uses ray-tracing to label points in the robot environment based on their dynamic properties. The network is composed of a 3D back-end that extracts rich features and enables the semantic segmentation of the lidar frames, and a 2D front-end that predicts the future information embedded in the SOGMs. We also design a navigation pipeline using these predicted SOGMs. We provide both quantitative and qualitative insights into the predictions and validate our choices of network design with an ablation study.

Keywords: Lifelong Learning, Self-Supervised, Occupancy Grid Maps

1 Introduction

Robot navigation, and particularly local planning, is complex in the presence of dynamic obstacles. Anticipating future motions has begun to be possible with recent advances in machine learning and robotics. In our work, we aim at providing an accurate prediction of the temporal evolution of the environment, enabling a robot to proactively plan efficient and safe trajectories. We advocate the use of Deep Neural Networks (DNN) to solve complex navigation tasks, through lifelong learning, as opposed to Reinforcement Learning (RL), which often replaces the whole navigation pipeline. Therefore we chose to rely on proven localization and planning algorithms, and focus our efforts on the bottleneck in the pipeline: predicting the future motions of the dynamic obstacles.

As opposed to object-centric methods, we chose to reduce the abstraction level and remain closer to the sensory data, by processing our input 3D lidar frames at the point level and providing predictions in the form of Occupancy Grid Maps (OGM), a discrete representation of the environment. Each grid cell contains an occupancy probability and is assumed to be independent from the others. We predict a set of OGM, one for each future time step, and call this representation Spatiotemporal Occupancy Grid Maps (SOGM) [1]. Note that this is different from the Dynamic Occupancy Grid Maps used by [2], which are OGM with additional velocity features in each cell.

We propose a novel feedforward network architecture able to predict SOGMs from 3D lidar frames (Figure 2). The network input consists of consecutive frames, aligned on a global map and merged, to provide both spatial and temporal information. Our network starts with a 3D back-end, processing the lidar frames with KPConv layers [3] to extract rich features that can be projected on a 2D grid or used for point cloud semantic segmentation. The 2D grid features are processed by a 2D front-end network outputting a SOGM. The characteristic of this 2D front-end is to be feedforward, without any recurrent connections. The occupancy predictions at consecutive time steps are computed by successive convolutions with independent weights. This enables our network to learn and predict a wider range of spatiotemporal patterns at different future horizons.

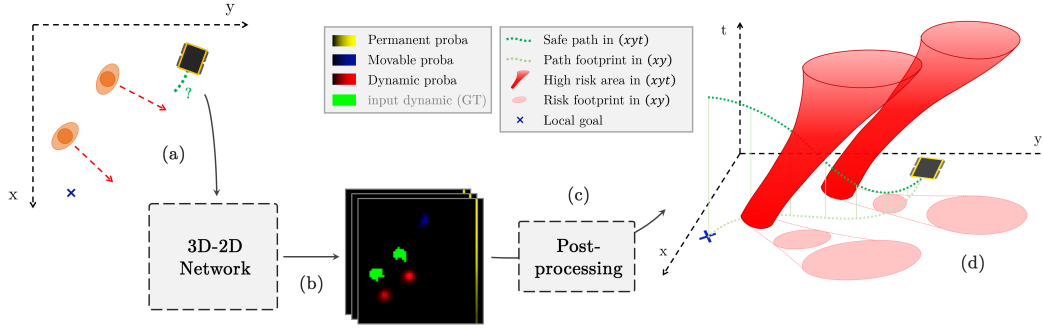


Figure 1: (a) The robot faces dynamic obstacles. (b) Our 3D-2D network computes occupancy probabilities for different obstacle classes. (c) The occupancy probabilities are processed into Spatiotemporal Risk Maps. (d) A local planner optimizes a trajectory in the 3D space (xyt) .

Our work is inspired by [4] that introduced a self-supervised pipeline for the segmentation of lidar frames. In this work, we use a similar automated annotation process with mapping and ray-tracing algorithms, providing four semantic labels to the lidar frames: *ground*, *permanent* (structures such as walls), *movable* (still-but-movable obstacles such as chairs), and *dynamic* (such as people). We add a SOGM generation algorithm, converting the annotated lidar frames to SOGMs. Therefore we are able to generate SOGMs with three channels, one for each type of obstacle: *permanent*, *movable*, and *dynamic*. To our knowledge, this had never been done and it allows a significant feature: our network can take into account interactions when predicting future motions. For example, dynamic obstacles will bounce off walls, avoid objects or pass through open doors.

Additionally, we worked on the integration of these SOGMs in the navigation stack. First, they are converted into Spatiotemporal Risk Maps (SRM), to reflect the risk of collision, linearly decreasing with the distance to occupied space. We modified the standard, Timed Elastic Band (TEB) [5, 6] local planner to handle SRMs. TEB normally optimizes a trajectory in a three-dimensional spatiotemporal space (x, y, t) , maximizing the distance to obstacles, so it only needs minor modifications to be adapted to minimize the risk value from the SRMs instead. We also keep the triaging idea from [4], with some improvements. We reduce the delay in localization by using the raw lidar frames to locate against the map and keep the advantage of triaging by updating the map only with classified frames. The main contributions of this paper are:

- An automated SOGM generation method using annotated lidar frames.
- A novel 3D-2D feedforward neural network predicting three-channel SOGMs.
- A proposed navigation system using SOGMs converted into SRMs.

In Section 3, we describe these contributions in details. In Section 4, we present our experiments and results, with a quantitative and qualitative analysis of the network SOGM predictions. In addition, we show an anecdotal example of our improved navigation system. All the experiments were performed in simulation¹.

2 Related Work

Navigation around dynamic obstacles has been studied for years. Early works [7, 8] tried to predict the future motion of pedestrians in videos, by learning a distribution of their possible trajectories. They used Inverse Optimal Control to recover a set of agent preferences consistent with prior demonstration. Following these preliminary works, several directions have been followed for dynamic obstacle forecasting.

Object tracking and trajectory prediction is a very common approach to enable motion planning in environments with dynamic obstacles. Following the success of recurrent neural network (RNN) and in particular long short-term memory networks (LSTM) for trajectory prediction [9, 10], the idea of isolating each obstacle as a distinct object has received a lot of attention. Katyal et al. [11] use an LSTM-based network to predict people trajectories and plan around them, while Peddi et al. [12] exploit a Hidden Markov Model to predict future states from a history of observations. In both

¹We plan on doing real-world experiments in crowded indoor spaces, but it is currently impossible due to covid-19 restrictions

cases, they rely on a detection and tracking algorithm. Similarly, Sathyamoorthy et al. [13] detect individual obstacles and predicts their speeds to avoid “freezing zones”. Similar object tracking and trajectory prediction techniques are also used in the context of autonomous driving [14, 15]. However, they all are dependent on the detection algorithm results and do not easily incorporate multi-modal predictions. In our work, we depart from these object-centric methods and provide spatiotemporal occupancy predictions.

The closest work to ours in this category predicts future human motions as 2D heat maps [16]. Therefore, they implicitly handle multi-modality like our method. However they still work at the object level, and like the OGM prediction methods below, their architecture is based on a recurrent network using 2D inputs, they do not include a 3D backbone network.

Reinforcement Learning has also been used extensively in recent years to replace standard motion planning algorithms [17, 18, 19, 20, 21, 22]. However, standard local planners have proven to be very reliable methods, especially when it comes to producing dynamically feasible trajectories, where most RL methods fail to do so. Even when the feasibility is ensured [23], the whole planning algorithm is embedded into a black box end-to-end neural network, which is difficult to tune and debug. We chose to keep a standard local planner, with its guarantees, and use a self-supervised deep learning method to predict the future motion of the dynamic obstacles.

OGM prediction is the line of study our work matches most closely. The distinction can be made between the handcrafted approaches [24, 24, 25, 26, 27] and the learned approaches [1, 28, 29, 16]. Handcrafted approaches usually rely on a model for human motion prediction. For example, Pierson et al. [24] predict a Dynamic Risk Density based on the occupancy density and velocity field of the environment. More recently, Huang et al. [30] extended this idea with a Gaussian Process regulated risk map of tracked pedestrians and cars. Other recent works focus on adapting the uncertainty of the predictive model [25, 26, 27]; they propose to use a real-time Bayesian framework in a closed-loop on real data. These methods either rely on object detection and tracking or are based on instantaneous velocities, and not able to predict future locations of obstacles accurately. Learned methods are closer to our work. Mohajerin and Rohani [29] introduce a difference-learning-based recurrent architecture to extract and incorporate motion information for OGM prediction. Schreiber et al. [28] present an LSTM-based encoder-decoder framework to predict the future environment represented as Dynamic Occupancy Grid Maps. They introduce recurrent skip connections into the network to reduce prediction blurriness. To account for the spatiotemporal evolution of the occupancy state of both static object and dynamic objects, Toyungyernsub et al. [1] propose a double-prong network architecture. However, if these methods are close to our work in the task they are trying to solve, their solution is very different from ours. They all take previous occupancy maps as inputs, effectively losing valuable information in the shape patterns that common 3D sensors can capture. On the contrary, we use consecutive 3D lidar scans as our input and keep a 3D network back-end able to capture both spatial and temporal patterns in the data. In addition, our network is able to make a distinction between different semantic classes including *dynamic* obstacles, long term *movable* objects and *permanent* structures, and to predict a future occupancy for each one of them. We also stress the fact that we do not need to include object detection or tracking, everything is processed at the point level in 3D lidar frames and the pixel level in the SOGMs.

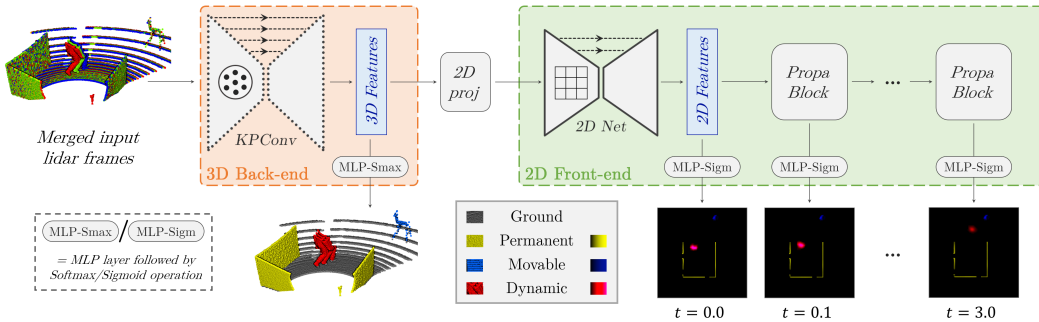


Figure 2: Illustration of our 3D-2D feedforward architecture. The 3D back-end is a 5-layer KPCnv architecture, producing features at the point level. The 2D front-end is composed of a 3-layer 2D U-Net architecture, followed by consecutive convolutional propagation blocks.

3 Risk-Aware Navigation System

This section describes our pipeline for the prediction of SOGMs and our navigation system design to make use of them. We first introduce the automated SOGM generation process, allowing our network to be trained using self-supervision. Then we detail our network architecture, shown in Figure 2, and the specifics of our network training and inference. Eventually, we present our risk-aware navigation system, with a modified TEB planner using SRMs.

3.1 Automated SOGM Generation

Generating the groundtruth SOGMs automatically for training is crucial to our pipeline. It allows us to train the network without human intervention, in a fully self-supervised manner. We follow the same lifelong learning principle as in [4]: data from previous navigation sessions can be used to train the network for new ones. Therefore, if the robot experiences new situations or new environments, our network can learn to deal with them.

Our automated generation process starts with the lidar frame segmentation, using the same parameters as [4]. A combination of a point cloud SLAM algorithm and a point cloud ray-tracing algorithm is used to create and then annotate a point cloud map for each previous navigation session. Four semantic labels are identified: *ground*, *permanent*, *movable*, and *dynamic*. These labels are projected back to the lidar frames of each session, which will be used to train the 3D semantic segmentation part of our network.

We provide additions to this automated annotation process, to generate SOGMs for the three obstacles classes: *permanent*, *movable*, and *dynamic*. Creating the SOGMs before the training of the network is not appropriate, because we want to use rotation augmentation, and rotating grid data is not trivial. Instead, we chose to precompute an intermediate spatiotemporal point cloud structure, which can easily be rotated and then transformed into SOGM during training. First, each annotated lidar frame is filtered to eliminate the ground points. We remove every point that is not annotated as one of the three labels listed above, or that is closer than 20 cm from the ground plane (found in an earlier step of the point cloud map annotation). Then we project all the points on the ground plane and subsample the obtained 2D point cloud with a grid size of 3cm. In addition to being easily rotated for data augmentation, this structure has the advantage to remain sparse compared to full grids.

At training time the precomputed future point clouds are loaded and stacked along a third dimension according to their timestamp. After being rotated for data augmentation, this spatiotemporal point cloud is projected to a SOGM structure of spatial resolution $dl_{2D} = 12\text{cm}$ and temporal resolution $dt = 0.1\text{s}$. The *permanent* and *movable* occupancy from all time steps of the SOGM are merged because they are not moving. Therefore, in addition to the future locations of dynamic obstacles, our network effectively learns to complete partially seen still objects. The SOGM generation process is illustrated in Figure 3.

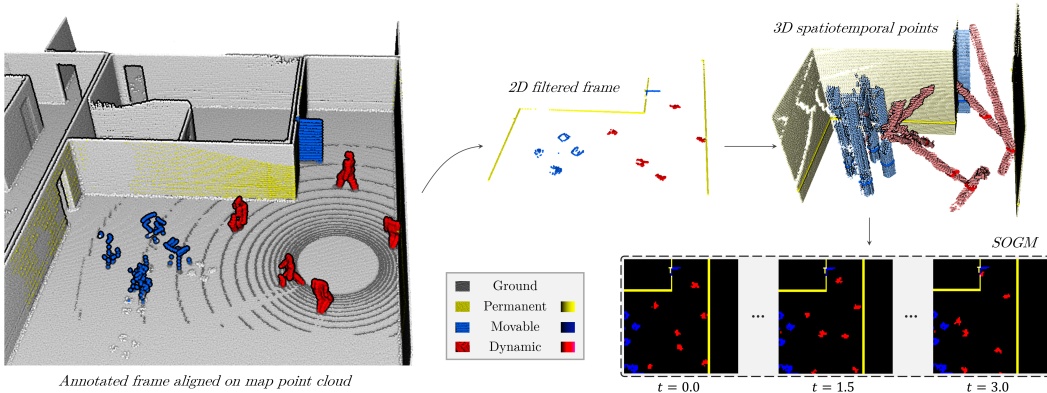


Figure 3: We generate SOGMs during training, using a 3D spatiotemporal point cloud structure made from 2D projections of the annotated lidar frames.

3.2 Network Architecture for SOGM Prediction

As shown in Figure 2, our network architecture is composed of two parts, a 3D back-end, and a 2D front-end. The 3D back-end is a KPConv convolutional neural network (CNN) [3] for point cloud semantic segmentation. We keep the KP-FCNN architecture and parameters of the original paper: a U-Net with five layers, each composed of two ResNet bottleneck-style blocks. This back-end network predicts semantic labels for the input point cloud. These predictions will be used for our improved triaging in the navigation system. Furthermore, they provide an additional supervising signal when training the network, which helps to extract rich 3D features. The network input is a point cloud made from $n_f = 3$ lidar frames aligned in the map coordinates and merged. We only keep the points inside a $R_{in} = 8m$ radius, as we are interested in the local vicinity of the robot. Each point is assigned a one-hot n_f -dimensional feature vector, encoding of the lidar frame it belongs to. Following the good practice advised in the KPConv paper, we control the input point cloud density with a grid subsampling ($dl_{3D} = 6cm$).

The 3D point features used to predict the semantic labels are also projected on a horizontal 2D grid with the same spatial resolution dl_{2D} as the SOGM. The size of the grid is determined as the inscribed square in the R_{in} -radius circle. Therefore the grid dimensions are:

$$h_{grid} = w_{grid} = \left\lceil \frac{R_{in} * \sqrt{2}}{dl_{2D}} \right\rceil \quad (1)$$

The features from the multiple points located in the portion of space, of a single grid cell are averaged. We tried using max-pooling instead, without any noticeable improvement. The features of the empty cells are set to zero.

The corresponding 2D feature map is then processed by our 2D front-end network. It starts with a common U-Net architecture with three layers, each composed of two ResNet bottleneck-style blocks. This part allows the network to diffuse the information contained in sparse locations, to the whole grid. The obtained feature map is used to predict the initial layer of the SOGM. Then, it is processed by successive propagation blocks, each composed of two ResNet bottleneck convolutions. The output of each propagation block is used to predict the corresponding layer of the SOGM. We define the final prediction time $T = 3.0s$, meaning that our SOGM dimensions are $h_{grid} = w_{grid} = 94$ and $d_{grid} = T/dt + 1 = 31$. Note that the *permanent* and *movable* predictions are redundant but we keep them to force the network to keep the knowledge of their location after the propagation blocks. It should help it to learn interactions between the classes further into the future.

3.3 Network Training and Inference

We define a particular training loss for our network:

$$L_{tot} = \lambda_1 L^{3D} + \lambda_2 \sum_{k < d_{grid}} \frac{L_k^{2D}}{d_{grid}} \quad (2)$$

where $\lambda_1 = 1.0$, $\lambda_2 = 10.0$, L^{3D} is the standard cross entropy loss for semantic segmentation with a KPConv network, and L_k^{2D} is the loss applied to layer k of our SOGM predictions:

$$L_k^{2D} = \sum_{i \in M_k} BCE(x_{k,i}, y_{k,i}) \quad (3)$$

where $x_{k,i}$ is the network logit at the pixel i of the time-step layer k in the SOGM, $y_{k,i}$ is its corresponding groundtruth and BCE is a Binary Cross-Entropy loss. Note that for clarity, we use a simple index i for 2D pixels. The SOGM loss is thus a masked Binary Cross-Entropy, where

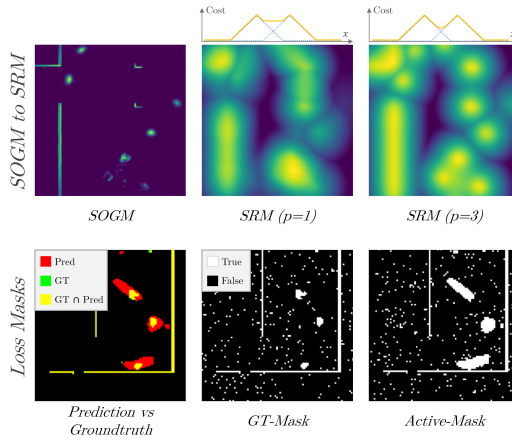


Figure 4: Top: conversion of SOGMs into SRMs. Bottom: Loss masks.

the mask M_k is here to help ignore the over-represented empty pixels and focus on the positive examples. We first tried a mask covering the positive groundtruth values in addition to some random pixels (GT-Mask), but then improved it to cover the union of positive groundtruth and positive prediction pixels (Active-Mask) to help reduce the false positives (See Figure 4 bottom).

Unless stated otherwise, we keep the same training parameters as in the original KPConv paper [3]. During training, we only use rotation augmentation around the vertical axis. With the parameters defined in the previous section, our input point clouds have on average 20,000 points. We use a variable batch size targeting $B = 6$, for an average of 85000 points per batch

3.4 Risk-Aware Navigation

We first transform our SOGMs into SRMs to encode the risk of collision instead of the occupancy probability. TEB originally minimizes a linearly decreasing cost function: $\mathcal{C}_{\text{obst}} = \max(0, 1 - d/d_0)$, where d is the distance to the closest obstacle and d_0 a predefined influence distance. We define a linearly decreasing risk value similarly:

$$\text{SRM}_{k,i} = \sum_j (\max(0, 1 - d(i,j) \times dl_{2D}/d_0)^p \times \text{SOGM}_{k,j})^{1/p} \quad (4)$$

where $d(i,j)$ is the distance from pixel i to pixel j in the grid space, d_0 is set to 2m. Like with a p -norm, when $p \rightarrow \infty$ this approximates the maximum of the linear influence of each surrounding pixel. When $p = 1$, this simply is the sum of the linear influence of each surrounding pixel, as shown in the top of Figure 4. We use $p = 3$ in the following, compute a SRM for each SOGM channel and keep the pixel-wise maximum. During optimization, the cost at a trajectory pose is defined as a bilinear interpolation of the SRM in space and time. If a pose time is too far in the future, it is ignored. TEB also allows the optimization of multiple trajectories for different homotopy classes. We keep this feature by creating fake point obstacles at local maxima in the SOGM, ignored by the optimizer, but used for homotopy class computation.

In addition, our network outputs a segmented point cloud, used to update the global planner 2D costmap, and the 3D point map for localization. We exclude the *dynamic* obstacles for the global planner and the *movable* and *dynamic* for the localization map. The localization is performed without delay with the raw lidar frames. For the modules depending on the network prediction, the delay is reasonable. On an Nvidia RTX 3090, our network forward pass takes less than 50ms with a CPU preprocessing of around 200ms. The SRM conversion takes about 30ms, if we add smaller other delays (communication for example), we end up with the first 3 or 4 layers of the SRM (out of 31) being obsolete, which is acceptable.

4 Experiments

4.1 Experimental Setup

We evaluate our method in a Gazebo simulated space, and we define three actor behaviors. **Bouncers** are more like marbles than humans, walking in straight lines and bouncing on every obstacle. **Wanderers** walk with a constant speed but randomly change direction. They also bounce off obstacles and are repelled by the robot. Eventually, **Flow Followers** are driven to a goal by a precomputed force field. They randomly choose their goal in a predefined set and only try to avoid the robot when it is very close to them.

For training our network, we create three different datasets, one for each behavior, and use randomized session setups. For each training set, we perform 18 sessions, including 3 for validation, with a random population, object count, and robot tour. At test time we can choose the robot objective and the population depending on the need of the experiment. As the space in this format is limited, we focus this experimental section on the evaluation of the network prediction and provide an anecdotal example of our navigation system using SRMs in the conclusion.

4.2 Quantitative Evaluation of the Network Predictions

We provide a quantitative analysis of the network results, including a comparison of the prediction performances for the different behaviors, and ablation studies for components of our network. We only evaluate the results for the *dynamic* class, which is the most significant. We thus have SOGM predictions (3D grids with values in $[0, 1]$), and binary groundtruth SOGM. We thus compute precision-recall curves and use Average Precision (AP) as our metric. AP can be obtained for a specific time step in the SOGM or the whole 3D grid.

First, we compare the results of the Bouncers, Wanderers, and Flow Followers experiments, by plotting AP for each time step in the SOGM (Figure 5). We see that the Bouncers and Wanderers start with similar performances, but, further in the future, the predictions become better for Bouncers. This is expected as the Bouncers walk straight, and are easier to predict than the Wanderers. Flow Followers are the most difficult to predict as their path is influenced by the force field, but also the other actors in the scene that they avoid, which is why the network struggles with them.

Then we focus on the Flow Followers dataset and evaluate our network in different configurations (Table 1). We evaluate the AP at 1.0s, 2.0s in the SOGM, and the overall AP of the 3D SOGM. We tested different architectures for the 2D front-end network. We define them with $(n_1-n_2-n_3)$, respectively the number of initial layers, the number of ResNet convolution per initial layer, and the number of ResNet convolution per propagation block. A deeper architecture gets better results but is also slower. We chose the (3-2-2) architecture for fast inference without losing much performance. We also show that the Active-Mask in our loss function is relevant, by comparing with the GT-Mask and no mask, both giving worse performances. We also show the importance of the 3D back-end to create rich features, by removing the 3D part of the loss ($\lambda_1 = 0$). Eventually, we tried to share the weights of the propagation blocks, effectively creating recurrent connections. The results are very bad because our architecture is not adapted for it. If we wanted to use recurrent connections, we should have used known powerful layers like LSTMs.

4.3 Qualitative Evaluation of the Network Predictions

It is hard to estimate the network performances through AP absolute values, especially because the multi-modal nature of the actor trajectories lowers these values. Consider a simple example: if a person faces three doors and chooses randomly where to go, we expect the network to predict that each trajectory is possible with a 33% probability, which automatically means at least 66% of false positives. In our case, the situations are more complex but the principle remains, which is why we need a thorough investigation of the qualitative results to assess the performances

We gathered noteworthy examples of SOGM predictions in Figure 6. The predictions are best seen when animated in the **supplementary video**, but here, we chose to show them a comprehensive format. First, we merged all the time steps of the SOGMs to see the movement that is predicted (a). We superimpose the groundtruth for the dynamic class as a trajectory, computed with a local maximum filter and colored from cyan to green for an indication of the temporal evolution.

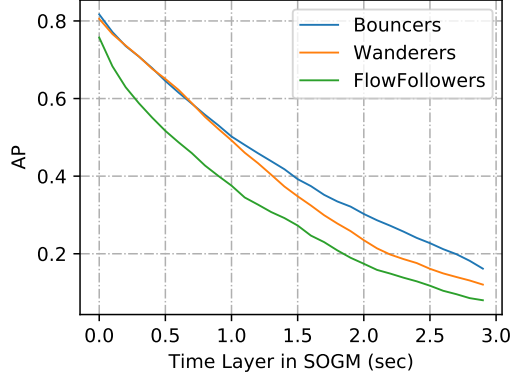


Figure 5: Comparison of the network performance for our three actor behaviors.

Table 1: Ablation study on Flow Followers.

	AP _{1.0}	AP _{2.0}	AP _{tot}
2DNet(4-4-3)	31.0%	11.5%	27.9%
2DNet(3-2-2)*	28.1%	8.9%	26.1%
2DNet(2-2-1)	23.7%	6.7%	23.8%
GT-Mask	25.6%	7.5%	24.5%
No Mask	25.7%	7.1%	23.0%
no-3D-loss	26.5%	8.0%	25.4%
shared-weights	3.6%	3.1%	7.9%

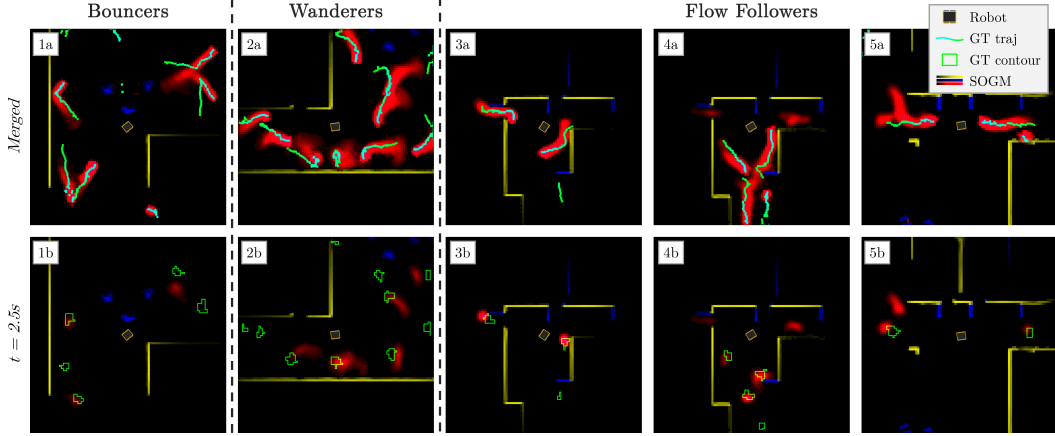


Figure 6: Examples of SOGM predictions. Time layers are merged in the top row too see temporal evolution, with superimposed groundtruth trajectories from cyan (start) to green (end). Bottom row shows a single time-step layer, with superimposed groundtruth in green.

We also show one layer of prediction 2.5 seconds into the future (b), with the groundtruth for the dynamic class superimposed as a contour. From left to right we can see several exciting results. First, the network handles Bouncers pretty well with accurate predictions even when they bounce on walls (1). It does not manage to predict bounces between actors, which is not surprising as this is less frequent and more random than wall bounces. Then we notice that the predictions for Wanderers generally have a shape similar to the banana distribution [31] (2b). The network is also able to predict that the Wanderers are repelled by the robot (2a). Flow Followers exhibit more complex trajectories, going through doors for example, that the network is able to predict (3). We observe an interesting phenomenon, the network often predicts a latent risk at some busy doorways (4), because during training the network often sees a person appearing there out of nowhere. Last but not least, our network sometimes predicts two possible trajectories, here one going through the door and one going straight (5), illustrating our point about multi-modal futures.

5 Conclusion and Future Work

In this paper, we presented a lifelong learning approach to make predictions for navigation in dynamic scenes, without the need to introduce object-level description. We showed that it was possible to generate SOGMs automatically and train a feedforward neural network to predict them in a self-supervised fashion. We evaluated the predicted SOGMs both quantitatively and qualitatively. We propose to use SOGMs in a navigation system, an example of which is shown in Figure 7. We reserve a thorough evaluation of this system and of the benefits of using SOGMs for future work, especially when real-world experiments will be possible again (hopefully very soon).

Following other works, we showed how self-supervision and lifelong learning are valuable for robotic navigation and hope that more work follows in this direction. There are many prospects for improvement, with more complex simulated human behaviors, and eventually real behaviors, by conditioning the SOGM predictions on the possible future robot actions, by combining recurrent and feed-forward architectures, or by including the notion of visible space in the generation and prediction of SOGMs.

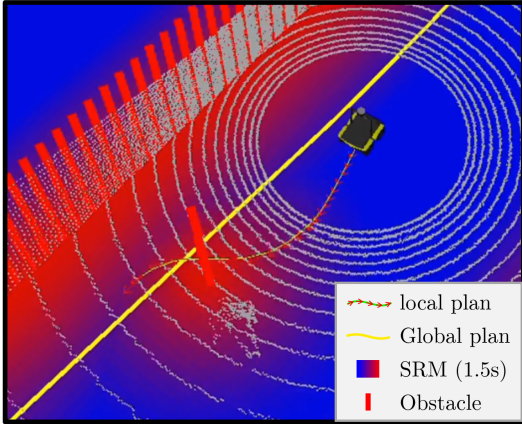


Figure 7: Proposed risk-aware navigation system. The local planner anticipates the actors future motion and plans to go behind them.

References

- [1] M. Toyungyernsub, M. Itkina, R. Senanayake, and M. J. Kochenderfer. Double-prong convlstm for spatiotemporal occupancy prediction in dynamic environments. *arXiv preprint arXiv:2011.09045*, 2020.
- [2] M. Schreiber, S. Hoermann, and K. Dietmayer. Long-term occupancy grid prediction using recurrent neural networks. In *2019 International Conference on Robotics and Automation (ICRA)*, pages 9299–9305. IEEE, 2019.
- [3] H. Thomas, C. R. Qi, J.-E. Deschaud, B. Marcotegui, F. Goulette, and L. J. Guibas. Kpconv: Flexible and deformable convolution for point clouds. In *Proceedings of the IEEE/CVF International Conference on Computer Vision*, pages 6411–6420, 2019.
- [4] H. Thomas, B. Agro, M. Gridseth, J. Zhang, and T. D. Barfoot. Self-supervised learning of lidar segmentation for autonomous indoor navigation. In *2021 IEEE International Conference on Robotics and Automation (ICRA)*. IEEE, 2021.
- [5] C. Rösmann, F. Hoffmann, and T. Bertram. Planning of multiple robot trajectories in distinctive topologies. In *2015 European Conference on Mobile Robots (ECMR)*, pages 1–6. IEEE, 2015.
- [6] C. Rösmann, F. Hoffmann, and T. Bertram. Integrated online trajectory planning and optimization in distinctive topologies. *Robotics and Autonomous Systems*, 88:142–153, 2017.
- [7] B. D. Ziebart, N. Ratliff, G. Gallagher, C. Mertz, K. Peterson, J. A. Bagnell, M. Hebert, A. K. Dey, and S. Srinivasa. Planning-based prediction for pedestrians. In *2009 IEEE/RSJ International Conference on Intelligent Robots and Systems*, pages 3931–3936. IEEE, 2009.
- [8] K. M. Kitani, B. D. Ziebart, J. A. Bagnell, and M. Hebert. Activity forecasting. In *European Conference on Computer Vision*, pages 201–214. Springer, 2012.
- [9] A. Alahi, K. Goel, V. Ramanathan, A. Robicquet, L. Fei-Fei, and S. Savarese. Social lstm: Human trajectory prediction in crowded spaces. In *Proceedings of the IEEE conference on computer vision and pattern recognition*, pages 961–971, 2016.
- [10] A. Gupta, J. Johnson, L. Fei-Fei, S. Savarese, and A. Alahi. Social gan: Socially acceptable trajectories with generative adversarial networks. In *Proceedings of the IEEE Conference on Computer Vision and Pattern Recognition*, pages 2255–2264, 2018.
- [11] K. D. Katyal, G. D. Hager, and C.-M. Huang. Intent-aware pedestrian prediction for adaptive crowd navigation. In *2020 IEEE International Conference on Robotics and Automation (ICRA)*, pages 3277–3283. IEEE, 2020.
- [12] R. Peddi, C. Di Franco, S. Gao, and N. Bezzo. A data-driven framework for proactive intention-aware motion planning of a robot in a human environment. In *2020 IEEE/RSJ International Conference on Intelligent Robots and Systems (IROS)*, pages 5738–5744. IEEE, 2020.
- [13] A. J. Sathyamoorthy, U. Patel, T. Guan, and D. Manocha. Frozone: Freezing-free, pedestrian-friendly navigation in human crowds. *IEEE Robotics and Automation Letters*, 5(3):4352–4359, 2020.
- [14] W. Luo, B. Yang, and R. Urtasun. Fast and furious: Real time end-to-end 3d detection, tracking and motion forecasting with a single convolutional net. In *Proceedings of the IEEE conference on Computer Vision and Pattern Recognition*, pages 3569–3577, 2018.
- [15] S. Casas, W. Luo, and R. Urtasun. Intentnet: Learning to predict intention from raw sensor data. In *Conference on Robot Learning*, pages 947–956. PMLR, 2018.
- [16] A. Jain, S. Casas, R. Liao, Y. Xiong, S. Feng, S. Segal, and R. Urtasun. Discrete residual flow for probabilistic pedestrian behavior prediction. In *Conference on Robot Learning*, pages 407–419. PMLR, 2020.
- [17] P. Long, T. Fan, X. Liao, W. Liu, H. Zhang, and J. Pan. Towards optimally decentralized multi-robot collision avoidance via deep reinforcement learning. In *2018 IEEE International Conference on Robotics and Automation (ICRA)*, pages 6252–6259. IEEE, 2018.

- [18] J. Liang, U. Patel, A. Sathiamoorthy, and D. Manocha. Crowdsteer: Realtime smooth and collision-free robot navigation in densely crowded scenarios trained using high-fidelity simulation. In *Proceedings of the Twenty-Ninth International Joint Conference on Artificial Intelligence, IJCAI*, volume 2020, pages 4221–4228, 2020.
- [19] A. J. Sathiamoorthy, J. Liang, U. Patel, T. Guan, R. Chandra, and D. Manocha. Densecavoid: Real-time navigation in dense crowds using anticipatory behaviors. In *2020 IEEE International Conference on Robotics and Automation (ICRA)*, pages 11345–11352. IEEE, 2020.
- [20] M. Everett, Y. F. Chen, and J. P. How. Collision avoidance in pedestrian-rich environments with deep reinforcement learning. *IEEE Access*, 9:10357–10377, 2021.
- [21] R. Strudel, R. Garcia, J. Carpentier, J.-P. Laumond, I. Laptev, and C. Schmid. Learning obstacle representations for neural motion planning. 2020.
- [22] L. Liu, D. Dugas, G. Cesari, R. Siegwart, and R. Dubé. Robot navigation in crowded environments using deep reinforcement learning. In *2020 IEEE/RSJ International Conference on Intelligent Robots and Systems (IROS)*, pages 5671–5677. IEEE, 2020.
- [23] U. Patel, N. K. S. Kumar, A. J. Sathiamoorthy, and D. Manocha. Dwa-rl: Dynamically feasible deep reinforcement learning policy for robot navigation among mobile obstacles. In *2021 IEEE International Conference on Robotics and Automation (ICRA)*. IEEE, 2020.
- [24] A. Pierson, C.-I. Vasile, A. Gandhi, W. Schwarting, S. Karaman, and D. Rus. Dynamic risk density for autonomous navigation in cluttered environments without object detection. In *2019 International Conference on Robotics and Automation (ICRA)*, pages 5807–5814. IEEE, 2019.
- [25] J. F. Fisac, A. Bajcsy, S. L. Herbert, D. Fridovich-Keil, S. Wang, C. J. Tomlin, and A. D. Dragan. Probabilistically safe robot planning with confidence-based human predictions. *arXiv preprint arXiv:1806.00109*, 2018.
- [26] A. Bajcsy, S. L. Herbert, D. Fridovich-Keil, J. F. Fisac, S. Deglurkar, A. D. Dragan, and C. J. Tomlin. A scalable framework for real-time multi-robot, multi-human collision avoidance. In *2019 international conference on robotics and automation (ICRA)*, pages 936–943. IEEE, 2019.
- [27] S. Bansal, A. Bajcsy, E. Ratner, A. D. Dragan, and C. J. Tomlin. A hamilton-jacobi reachability-based framework for predicting and analyzing human motion for safe planning. In *2020 IEEE International Conference on Robotics and Automation (ICRA)*, pages 7149–7155. IEEE, 2020.
- [28] M. Schreiber, V. Belagiannis, C. Gläser, and K. Dietmayer. Motion estimation in occupancy grid maps in stationary settings using recurrent neural networks. In *2020 IEEE International Conference on Robotics and Automation (ICRA)*, pages 8587–8593. IEEE, 2020.
- [29] N. Mohajerin and M. Rohani. Multi-step prediction of occupancy grid maps with recurrent neural networks. In *Proceedings of the IEEE/CVF Conference on Computer Vision and Pattern Recognition*, pages 10600–10608, 2019.
- [30] Z. Huang, W. Schwarting, A. Pierson, H. Guo, M. Ang, and D. Rus. Safe path planning with multi-model risk level sets. In *2020 IEEE/RSJ International Conference on Intelligent Robots and Systems (IROS)*, pages 6268–6275. IEEE, 2020.
- [31] A. W. Long, K. C. Wolfe, M. J. Mashner, and G. S. Chirikjian. The banana distribution is gaussian: A localization study with exponential coordinates. *Robotics: Science and Systems VIII*, 265, 2013.